

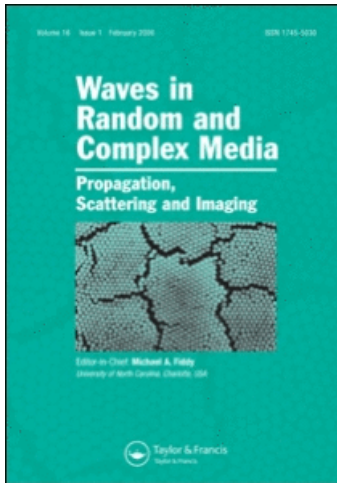
This article was downloaded by: [Goray, Leonid Ivanivich]

On: 15 November 2010

Access details: Access Details: [subscription number 929642966]

Publisher Taylor & Francis

Informa Ltd Registered in England and Wales Registered Number: 1072954 Registered office: Mortimer House, 37-41 Mortimer Street, London W1T 3JH, UK



Waves in Random and Complex Media

Publication details, including instructions for authors and subscription information:

<http://www.informaworld.com/smpp/title~content=t716100762>

Application of the boundary integral equation method to very small wavelength-to-period diffraction problems

L. I. Goray^{ab}

^a Saint Petersburg Academic University, Khlopina 8/3, 194021 Russian Federation ^b Institute for Analytical Instrumentation, RAS, Rizhsky Pr. 26, 190103 Russian Federation

Online publication date: 15 November 2010

To cite this Article Goray, L. I.(2010) 'Application of the boundary integral equation method to very small wavelength-to-period diffraction problems', *Waves in Random and Complex Media*, 20: 4, 569 — 586

To link to this Article: DOI: 10.1080/17455030.2010.510857

URL: <http://dx.doi.org/10.1080/17455030.2010.510857>

PLEASE SCROLL DOWN FOR ARTICLE

Full terms and conditions of use: <http://www.informaworld.com/terms-and-conditions-of-access.pdf>

This article may be used for research, teaching and private study purposes. Any substantial or systematic reproduction, re-distribution, re-selling, loan or sub-licensing, systematic supply or distribution in any form to anyone is expressly forbidden.

The publisher does not give any warranty express or implied or make any representation that the contents will be complete or accurate or up to date. The accuracy of any instructions, formulae and drug doses should be independently verified with primary sources. The publisher shall not be liable for any loss, actions, claims, proceedings, demand or costs or damages whatsoever or howsoever caused arising directly or indirectly in connection with or arising out of the use of this material.

Application of the boundary integral equation method to very small wavelength-to-period diffraction problems

L.I. Goray^{a,b*}

^a*Saint Petersburg Academic University, Khlopina 8/3, St. Petersburg, 194021 Russian Federation;* ^b*Institute for Analytical Instrumentation, RAS, Rizhsky Pr. 26, St. Petersburg, 190103 Russian Federation*

(Received 25 March 2009; final version received 19 July 2010)

Diffraction from 1D multilayer gratings having arbitrary border profiles including edges is considered for small wavelength-to-period (λ/d) ratios, the most difficult case for any rigorous numerical method. The boundary integral equation theory is so flexible that we can indicate a few areas where it can be modified. In this work, special attention is paid to the main aspects of the Modified Boundary Integral Equation Method for $\lambda/d \ll 1$ as well as to a more general treatment of the energy conservation law applicable to multilayer absorption gratings. Three types of small λ/d problems are known from optical applications: (a) shallow gratings working in the X-ray and extreme ultraviolet ranges, both at near-normal and grazing angles, (b) deep echelle gratings with a steep working facet illuminated along its normal by light of any wavelength, and (c) rough mirrors and gratings in which rough boundaries can be represented by a large- d grating, and which contain a number of random asperities illuminated at any angle and wavelength. Numerical examples of diverse in-plane diffraction problems are presented.

1. Introduction

This work is part of the research that has been pursued over a long period of time with the purpose of developing accurate and fast numerical algorithms, including commercial packages, designed to work in all, including the shortest, wavelength ranges [1–3]. Diffraction from 1D multilayer gratings with arbitrary border profiles, including edges and random roughnesses, is considered in the in-plane (classical) mount. A more general case of the off-plane (conical) mount will be addressed in future publications. The term ‘1D multilayer’ refers to a general 1D grating or rough mirror on a planar surface of arbitrary conductivity which is periodic in one direction, constant in the second, and has a finite number of borders and layers in the third. The actual number of identical or different borders and layers can be large enough, up to a few thousand for hard X-ray applications. Though various approximated analyses [4,5] developed for the treatment of such challenging diffraction problems enjoy more or less successful application, they are always

*Email: lig@skylink.spb.ru

plagued with uncertainties which make comparison between rigorous and non-rigorous approaches difficult.

The boundary integral equation theory is so flexible that we can indicate a few areas where it can be modified [6,7]. They are: (1) physical model (choice of boundary types and conditions); (2) mathematical structure (integral representations using potentials or integral formulas and a multilayer scheme); (3) method of discretization (choice of basis and trial functions, discretization scheme and treatment of corners in boundary profile curves); (4) low-level details (calculations and optimization of Green's functions and their derivatives (Green's series), mesh of sample (collocation) points, quadrature rules, solution of linear systems, caching of repeating quantities, etc.). A self-consistent explanation of various integral methods is well beyond the scope of this study, and one should rather be addressed to the references at the end of the paper. In this work, special attention is paid to all aspects of the Modified Boundary Integral Equation Method (MIM) for small wavelength-to-period ratios ($\lambda/d \ll 1$) as well as to a more general treatment of the energy conservation law applicable to multilayer absorption gratings. Two different solvers based on the MIM are used in the present work to analyze the diffractive properties of bulk and multilayer gratings with arbitrary angles of incidence, boundary shapes, and layer thicknesses, including non-conformal layers and real-profile boundaries. Numerical examples of diverse problem types are presented.

2. Theory

2.1. Diffraction problem

The multilayer grating is a stack of cylindrical surfaces whose generatrices are parallel to the z -axis and whose section in the (x, y) -plane is given by simple, non-intersecting and d -periodic curves $\Sigma_j, j = 0, \dots, N-1$, either C^∞ or piecewise C^2 (see Figure 1). We assume that the open arc Γ_j denotes one period of Σ_j . The y projections of the boundaries are to be overlapping or not; it depends on the

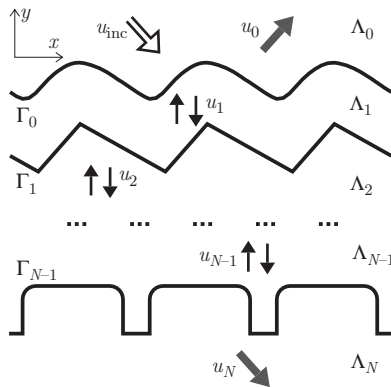


Figure 1. Schematic cross-section of a grating.

multilayer scheme used (cf. the next subsection). Consider a multilayer structure consisting of $N + 1$ homogeneous material layers $\Lambda_0, \dots, \Lambda_N$ characterized by their refractive indices v_j so that $v_j^2 = \varepsilon_j \mu_j, j = 0, \dots, N$ with piecewise constant functions of electric permittivity and magnetic permeability $\varepsilon(x, y) = \varepsilon_j$ and $\mu(x, y) = \mu_j$, respectively. One refers to the semi-infinite top Λ_0 and bottom Λ_N layers. It is assumed that the light incident from Λ_0 in the $y0x$ plane with the vacuum wavelength λ and pulsance ω has the time dependence $e^{-i\omega t}$. Because additionally Σ_j is not varying in the z direction, it is possible to deal with the two fundamental cases of polarization separately, i.e. the TE mode (with the z component E_z^{inc} of the electric field \mathbf{E}_{inc} parallel to the grating grooves) and the TM mode (with the z component H_z^{inc} of the magnetic field \mathbf{H}_{inc} parallel to the grating grooves) [8]. Thus, the original three-dimensional (3D) diffraction problem reduces to a 2D one and becomes independent of the z direction of the grating:

$$\begin{aligned} u_{\text{inc}}(x, y) &= E_z^{\text{inc}}(x, y)e^{i(\alpha x - \beta y)} \quad (\text{TE}), \\ u_{\text{inc}}(x, y) &= H_z^{\text{inc}}(x, y)e^{i(\alpha x - \beta y)} \quad (\text{TM}), \end{aligned} \tag{1}$$

where $\alpha = k_0 \sin \theta_{\text{inc}}$ and $\beta = k_0 \cos \theta_{\text{inc}} > 0$ with the incident wavenumber $k_0 = 2\pi v_0 / \lambda$ and $|\theta_{\text{inc}}| < \pi/2$. The wavevectors \mathbf{k}_j for $(x, y) \in \Lambda_j$ in medium number $j \geq 1$ satisfy $k_j^2 = k_0^2 (v_j / v_0)^2$. Due to the periodicity of Σ_j the incident wave is scattered into a finite number of plane waves in $\Lambda_0 \times \mathbb{R}$ and also in $\Lambda_N \times \mathbb{R}$ if k_N is real.

The induced field inside the layer j is denoted $u_j(x, y), j \geq 1$. Also for $j = 0, \dots, N - 1$ define the functions on the boundaries:

$$\begin{aligned} u_j^+ &= u_j|_{\Gamma_{j-1}}, \quad v_j^+ = \partial_n u_j|_{\Gamma_{j-1}}, \\ u_j^- &= u_j|_{\Gamma_j}, \quad v_j^- = \partial_n u_j|_{\Gamma_j}, \end{aligned} \tag{2}$$

where $\partial_n = n_x \partial_x + n_y \partial_y$ denotes the normal derivative on Γ_j and $v_{\text{inc}} = \partial_n u_{\text{inc}}$. Thus, there are four values attributed to every boundary Γ_j : the *upper* values u_j^-, v_j^- (that belong to the layer Λ_j and are the *floor* values for that layer), and the *lower* values u_{j+1}^+, v_{j+1}^+ (that belong to the layer Λ_{j+1} and are the *ceiling* values for that layer).

Taking into account the continuity of the tangential components of the total field on the surfaces we can write the jump (transmission) conditions for these four values in the form

$$\begin{bmatrix} u_j^- \\ v_j^- \end{bmatrix} + \delta_{j0} \begin{bmatrix} u_{\text{inc}} \\ v_{\text{inc}} \end{bmatrix} = B_j \begin{bmatrix} u_{j+1}^+ \\ v_{j+1}^+ \end{bmatrix}, \tag{3}$$

where δ_{j0} is the Kronecker symbol. Here the matrix $B = \text{Diag}(1, \rho_j)$ is a 2×2 diagonal matrix with $\rho_j = \mu_j / \mu_{j+1}$ or $\rho_j = \varepsilon_j / \varepsilon_{j+1}$ for the TE or the TM polarization, respectively. In this form, the conditions hold also for a perfectly conducting bottom layer and in the conical case [9].

The Maxwell equations imply that the total field in all regions $\Lambda_j, j = 0, \dots, N$ excluding all boundaries $\Gamma_j, j = 0, \dots, N - 1$ satisfy the scalar Helmholtz equation

$$(\Delta + k_j^2) u_{\text{tot}}(x, y) = 0, \tag{4}$$

where $u_{\text{tot}}(x, y)$ are the z -components of the total electric, respectively, magnetic field.

The z -components of the incoming field are α -quasiperiodic in x of period d , i.e. they satisfy the relation

$$u_{\text{inc}}(x + d, y) = e^{id\alpha} u_{\text{inc}}(x, y).$$

In view of the periodicity of ε_j and μ_j this motivates us to seek α -quasiperiodic solutions $u_{0,N}$. Furthermore, the diffracted field must remain bounded at infinity, which implies the well-known outgoing wave conditions (the Sommerfeld radiation conditions) represented in the form of the Rayleigh expansion in the far field with complex reflection c_m^- and transmission c_m^+ order amplitudes) in the upper ($-$) and lower ($+$) media

$$\begin{aligned} u_{\text{tot}}(x, y) &= u_{\text{inc}} + \sum_{n \in \mathbb{Z}} c_m^- e^{i(\alpha_m x + \beta_m^- y)}, \quad y \geq 0; \\ u_N(x, y) &= \sum_{n \in \mathbb{Z}} c_m^+ e^{i(\alpha_m x - \beta_m^+ y)}, \quad y \leq -H, \end{aligned} \tag{5}$$

where $\Sigma_j \subset \{(x, y) : y < 0 \wedge |y| < H\}$ and α_m , for the order number m are given by relations

$$\alpha_m = \alpha + \frac{2\pi m}{d}, \quad (\beta_m^j)^2 = k_j^2 - \alpha_m^2, \quad \beta_m^\mp = \beta_m^{0,N}, \quad 0 \leq \arg \beta_m^\mp < \pi.$$

In the following it is also assumed that

$$\arg \varepsilon_j \geq 0, \quad \arg \mu_j \leq \pi, \quad \arg(\varepsilon_j \mu_j) < 2\pi,$$

which holds for all existing optical (meta)materials [9]. Then $0 \leq \arg k_N^2 < 2\pi$ and β_m^+ are properly defined for all m .

2.2. Boundary potentials, integral equations, and multilayer schemes

The integral equation approach of the present paper transforms the problem (1)–(5) into a system of integral equations over profile curves. We combine here the direct and indirect approaches as proposed in [8,10]. The multilayer scheme in our solver is the original one of Maystre, that is, variant D in each layer by Pomp’s classification ([10], p. 113). The functions u_j^\mp, v_j^\mp are represented using the upper and lower limits of the single and double layer potentials with unknown densities φ_j on Γ_j of single layer potentials defined on the layer ceilings

$$\begin{aligned} V_{\Gamma_j, k_j}^\mp \varphi_j(P) &= \int_{\Gamma_j} \varphi_j(Q) \Psi_{k_j, \alpha}(P - Q) d\sigma_Q, \\ W_{\Gamma_j, k_j}^\mp \varphi_j(P) &= \int_{\Gamma_j} \varphi_j(Q) \partial_n(Q) \Psi_{k_j, \alpha}(P - Q) d\sigma_Q, \end{aligned} \tag{6}$$

where $\Psi_{k_j, \alpha}(P)$, $P=(X, Y)$, is the quasiperiodic fundamental solution of period d (Green’s function) given by the infinite series

$$\frac{i}{4} \sum_{m=-\infty}^{\infty} H_0^{(1)}\left(k_j \sqrt{(X - md)^2 + Y^2}\right) e^{imd\alpha} = \frac{i}{2d} \sum_{m=-\infty}^{\infty} \frac{e^{i(\alpha_m X + \beta_m^j Y)}}{\beta_m^j},$$

where $H_0^{(1)}$ is the first Hankel function of order zero. In Equation (6) $d\sigma_Q$ denotes integration with respect to the arc length and $n(Q)$ is the normal to Γ_j at $Q \in \Gamma_j$ pointing into Λ_j .

The value of the field in the layers can be found using the boundary data and the famous Green’s formula. Then, a down-up marching procedure can be applied using recurrence formulas for φ_n and initial values $u_{0,N}$ and $v_{0,N}$ [1]. For the top layer we can obtain the boundary integral equation with respect to φ_1 (cf. Equation (41) in [1])

$$\{(I + W_0^-)Y_1 - V_0^- \rho_0^{-1} Z_1\} \varphi_1 = (I + W_0^-)u_{inc} - V_0^- v_{inc}, \tag{7}$$

where expressions for the operators Y_j and Z_j can be found in [1] (Equations (34) and (38), respectively). If the bottom layer is perfectly conducting, the recurrence terminates at φ_N .

The choice of a numerical method to solve the multi-boundary integral equations is to a large extent independent of other implementation details of the single-boundary algorithm. It is not even necessary to use the same method for every boundary provided that adjacent boundary solvers have a common data interface. There are two different multilayer solvers implemented in the present code. The ‘Separating’ multi-boundary solver is based on the scattering amplitude matrix algorithm [11]. By definition, it requires that a homogeneous medium separates two adjacent corrugated regions by fictitious planes. The ‘Penetrating’ multi-boundary solver is based on the algorithm described in [1,2] and does not require a separation between two adjacent corrugated regions. A more transparent and detailed exposition, including a discussion of various marching schemes that avoid hypersingular potential operators, is given in [1,10]. Analytical aspects of boundary integral operators can be found in many sources (cf. e.g. [9,10,12,13]).

2.3. Efficiency, absorption, and energy balance

Diffraction efficiencies or far field patterns for the reflected and transmitted fields can easily be found from the corresponding boundary values. The efficiency of a diffracted order represents the proportion of power radiated in each order. Defining the power as the flux of the modulus of the Poynting vector $|\mathbf{S}^{inc}| = \text{Re}(\mathbf{E}^{inc} \times \mathbf{H}^{inc})/2$ (\bar{A} denotes the complex conjugate of A) through a normalized rectangle parallel to the (x, z) -plane, the ratio of the power of a reflected or transmitted propagating order and of the incident wave gives the diffraction efficiency η_m^\mp of this order for the partially polarized incident light in the form:

$$\begin{aligned} \eta_m^- &= (\beta_m^-/\beta) (|c_m^-(TE)|^2 \sin^2 \delta + |c_m^-(TM)|^2 \cos^2 \delta), \\ \eta_m^+ &= (\beta_m^+/\beta) (v_0/v_N)^2 (|c_m^+(TE)|^2 \sin^2 \delta + |c_m^+(TM)|^2 \cos^2 \delta), \end{aligned} \tag{8}$$

where the incident and diffracted plane waves are given by the polarization angle $\delta = \arctan[|E_z^{\text{inc}}| / |H_z^{\text{inc}}|]$ with the normalization $|E_z^{\text{inc}}|^2 + |H_z^{\text{inc}}|^2 = 1$.

One of the most important accuracy criteria based on a single computation is the energy balance that can be generalized in the lossy multilayer case described below. If the grating is perfectly conducting, then the conservation of energy is expressed by the standard energy criterion

$$R = 1, \quad (9)$$

where R is the sum of the reflection order efficiencies.

If the grating is lossless, $\text{Im } v_j = 0, j = 0, \dots, N$, then conservation of energy is expressed by a similar energy criterion

$$R + T = 1, \quad (10)$$

where T is the sum of the transmission order efficiencies.

In the general case,

$$A + R + T = 1, \quad (11)$$

where A is called the absorption coefficient or simply the absorption in the given diffraction problem. Besides being physically meaningful, expression (11) is very useful as a numerical accuracy test for computational codes and especially important in the X-ray and EUV ranges, where absorption plays a predominant role. In the lossy case, one needs an independently calculated quantity A to verify Equation (11). For such a quantity, we use the absorption integrals defined in [2] and derived below.

Because of the problem being invariant under translation by an integer number of periods along the axis perpendicular to the grooves, one may restrict oneself to an analysis of the heat power loss \tilde{E}_A per grating period. \tilde{E}_A can be calculated as the difference between the energy fluxes that have crossed the upper, Γ_0 , and the lower, Γ_{N-1} , boundaries of the multilayer structure through an element of area bounded by the $x = 0, x = d, z = 0$, and $z = 1$ planes:

$$\tilde{E}_A = \int_0^1 dz \int_{\Gamma_0} \mathbf{S}_0^+ \mathbf{n}_0 ds - \int_0^1 dz \int_{\Gamma_{N-1}} \mathbf{S}_{N-1}^+ \mathbf{n}_{N-1} ds, \quad (12)$$

where \mathbf{S}_0^+ and \mathbf{S}_{N-1}^+ are time-averaged complex Poynting vectors calculated at the upper and lower boundaries, \mathbf{n}_0 and \mathbf{n}_{N-1} are unit vectors of the normal, which are interior to the regions under study, and arc length integration is performed along the cut of the boundaries by the $z = 0$ plane.

Recalling that $|\mathbf{S}_j^+| = 0.5 \text{Re } \mathbf{E}_j^+ \times \overline{\mathbf{H}_j^+}$ we open the vector and dot products for the TE and TM polarizations under the integral signs in Equation (12):

$$\begin{aligned} \tilde{E}_A^{\text{TE}} &= 0.5 \text{Re} \left[\int_{\Gamma_0} E_z^+ (\overline{H_x^+} \cos b - \overline{H_y^+} \cos a) ds - \int_{\Gamma_{N-1}} E_z^+ (\overline{H_x^+} \cos b - \overline{H_y^+} \cos a) ds \right], \\ \tilde{E}_A^{\text{TM}} &= 0.5 \text{Re} \left[\int_{\Gamma_0} \overline{H_z^+} (E_x^+ \cos b - E_y^+ \cos a) ds - \int_{\Gamma_{N-1}} \overline{H_z^+} (E_x^+ \cos b - E_y^+ \cos a) ds \right]. \end{aligned} \quad (13)$$

As follows from Maxwell's equations

$$\begin{aligned} \partial_n \overline{E_z^+} &= (-\overline{H_y^+} \cos a + \overline{H_x^+} \cos b) / (i\omega\mu_j), \\ \partial_n H_z^+ &= (-E_y^+ \cos a + E_x^+ \cos b) / (i\omega\epsilon_j). \end{aligned} \tag{14}$$

Substituting Equation (14) in Equation (13), we obtain

$$\begin{aligned} \tilde{E}_A^{\text{TE}} &= 0.5 \operatorname{Re} \left[\int_{\Gamma_0} \frac{1}{i\omega\mu_1} \partial_n \overline{E_z^+} E_z^+ \, ds - \int_{\Gamma_{N-1}} \frac{1}{i\omega\mu_N} \partial_n \overline{E_z^+} E_z^+ \, ds \right], \\ \tilde{E}_A^{\text{TM}} &= 0.5 \operatorname{Re} \left[\int_{\Gamma_0} \frac{1}{i\omega\epsilon_1} \partial_n H_z^+ \overline{H_z^+} \, ds - \int_{\Gamma_{N-1}} \frac{1}{i\omega\epsilon_N} \partial_n H_z^+ \overline{H_z^+} \, ds \right]. \end{aligned} \tag{15}$$

In studies of electromagnetic field losses at the grating, \tilde{E}_A , it should be normalized against the heat power losses of the incident wave, E_A , within a plane element of area bounded by the same planes $x=0$, $x=d$, $z=0$, and $z=1$:

$$\begin{aligned} E_A^{\text{TE}} &= 0.5 \operatorname{Re} \left[\int_0^d \frac{1}{i\omega\mu_1} \partial_n \overline{E_z^{\text{inc}}} E_z^{\text{inc}} \, dx \right], \\ E_A^{\text{TM}} &= 0.5 \operatorname{Re} \left[\int_0^d \frac{1}{i\omega\epsilon_1} \partial_n H_z^{\text{inc}} \overline{H_z^{\text{inc}}} \, dx \right]. \end{aligned} \tag{16}$$

By canceling the same factor $e^{i\alpha x}$ in the expressions for the incident and diffracted fields in a diffraction problem the explicit form of the incident field of unit amplitude and of its normal derivative can be simplified:

$$\begin{aligned} E_z^{\text{inc}}, H_z^{\text{inc}} &= e^{-i\beta y}, \\ \partial_n E_z^{\text{inc}}, \partial_n H_z^{\text{inc}} &= e^{-i\beta y} (-i\beta). \end{aligned} \tag{17}$$

Substituting now Equation (17) into Equation (16), recalling the boundary conditions, and taking account of the plane surface of integration, we come to

$$\begin{aligned} E_A^{\text{TE}} &= 0.5\beta d / \omega\mu_0, \\ E_A^{\text{TM}} &= 0.5\beta d / \omega\epsilon_0. \end{aligned} \tag{18}$$

Using Equation (15) in conjunction with Equation (18), the normalized expressions for \tilde{E}_A , the electromagnetic field energy absorbed in the multilayer grating, transform to

$$\begin{aligned} A^{\text{TE}} &= \frac{\tilde{E}_A^{\text{TE}}}{E_A^{\text{TE}}} = \frac{1}{\beta d} \operatorname{Re} \left[\int_{\Gamma_0} \frac{i\mu_0}{\mu_1} \partial_n \overline{E_z^+} E_z^+ \, ds - \int_{\Gamma_{N-1}} \frac{i\mu_0}{\mu_N} \partial_n \overline{E_z^+} E_z^+ \, ds \right], \\ A^{\text{TM}} &= \frac{\tilde{E}_A^{\text{TM}}}{E_A^{\text{TM}}} = \frac{1}{\beta d} \operatorname{Re} \left[\int_{\Gamma_0} \frac{i\epsilon_0}{\epsilon_1} \partial_n H_z^+ \overline{H_z^+} \, ds - \int_{\Gamma_{N-1}} \frac{i\epsilon_0}{\epsilon_N} \partial_n H_z^+ \overline{H_z^+} \, ds \right]. \end{aligned} \tag{19}$$

Recalling that $\text{Re } X = \text{Im } iX$, Equation (19) for the universal field components u_j^\mp and their normal derivatives v_j^\mp can be recast into the form

$$A = \frac{1}{\beta d} \text{Im} \left[\int_{\Gamma_0} u_0^- \overline{v_0^-} ds - c \int_{\Gamma_{N-1}} u_N^+ \overline{v_N^+} ds \right], \quad (20)$$

where $c = \mu_0/\mu_N$ for the TE, and $c = \varepsilon_0/\varepsilon_N$, for the TM polarization.

Equation (20) for the absorption A of an electromagnetic field by a multilayer grating coincides with the expression reported in [2] and derived by applying the second Green's identity to boundary functions for the contours in the upper and lower media. By definition, the first integral in Equation (20) is $1 - R$, and the second, T , vanishes if the lower medium is absorbing [15] or the lower boundary is perfectly conducting. The sum $A + R + T$ is actually the energy balance for an absorbing grating, and the extent to which it approaches unity is a measure of the accuracy of a calculation.

3. Modifications of the theory and implementation

It is well known that solution of the 2D Helmholtz equation with any rigorous numerical code meets with difficulties at small λ/d [12,14,16–20]. While the Standard Boundary Integral Equation methods (SIMs) are robust, reliable, and efficient, they exhibit poor convergence and loss of accuracy in the high-frequency range due to numerical contamination in quadratures. Increasing matrix size and enhancing computation precision, as well as application of convergence speed-up techniques, which are successfully explored in low- and mid-frequency ranges, lead to unreasonably stringent requirements for computing times and storage capacities in high and, especially, ultrahigh frequency ranges ($\lambda/d < 1.E-2$ and $\lambda/d < 1.E-3$). This section addresses a number of modifications required for the SIM to transform it to the MIM together with relevant discussions.

3.1. Multilayer and discretization schemes

As to the implemented multilayer schemes, there are no substantial differences between the well established approaches and the MIM in these higher levels of the multilayer boundary integral equation theory.

In practice, the convergence and accuracy of efficiency computation depend significantly on a proper choice of the discretization scheme and of the quadrature rule for the SIMs [12]. Usually, one of collocation methods (Method of Moments) is used with the distribution of points on a uniform grid. In low- and mid-frequency ranges, better results are often obtained using equidistant steps along the arc length [13,18,21]. Another possible function of the distance between collocation points is prescribed by equal steps along the axis perpendicular to the grooves [6,8]. As pointed out in [8], in the case of regular kernels and periodic integrand functions, a step function approximation of the integrand expression, with division of the integration interval (period) into equal parts, is preferable. In the MIM, the fastest Nyström method is used (cf. [2]), where the integrals in the integral operators are

approximated by the quadrature rule with the collocation points used as quadrature knots. Such a direct discretization method combined with the simplest rectangle (trapezium) integration rule works well for shallow border profile gratings and, especially, at small λ/d [1,3,15]. In the presence of a profile with corners (piecewise linear), the collocation and quadrature nodes are set in such a way that every corner lies half-way between the nodes adjacent to it and no curvature-like single-term corrections are added [3,15]. However, for deep grating calculations another version of the quadrature formula involving the normal derivative of the Green's function should be used. The nodes are set in such a way that all corners are nodes and the curvature corrections are applied by adding the corner term [6]. A more efficient approach with meshes of collocation points graded towards the corner points of the profile curves together with the appropriated quadrature rule is introduced in [12].

3.2. Numbers of collocation points required in the SIM and MIM

It is well known that the number of collocation points per wavelength used in the various SIMs can be reduced significantly, up to an order of magnitude, when λ/d becomes small [3,8,19]. The question is how small it might be for very small λ/d problems, say for $\lambda/d < 1.E-3$?

In Figures 2 and 3, convergence of the SIM is demonstrated for an analytical case of diffraction from a plane transmission interface (normal incidence in vacuum with the lower-medium refractive index $n_1=1.5$) for different λ/d . For $\lambda/d=1$ in Figure 2(a), the convergence rate reached with speed-up techniques is high, with the energy balance error of $\sim 1.E-6$ in both polarization states for the number of collocation points $\tilde{N}=10$. For $\lambda/d=1.E-1$ in Figure 2(b), the convergence rate reached with speed-up techniques is medium, with the energy balance error of $\sim 1.E-5$ in both polarizations for $\tilde{N}=100$.

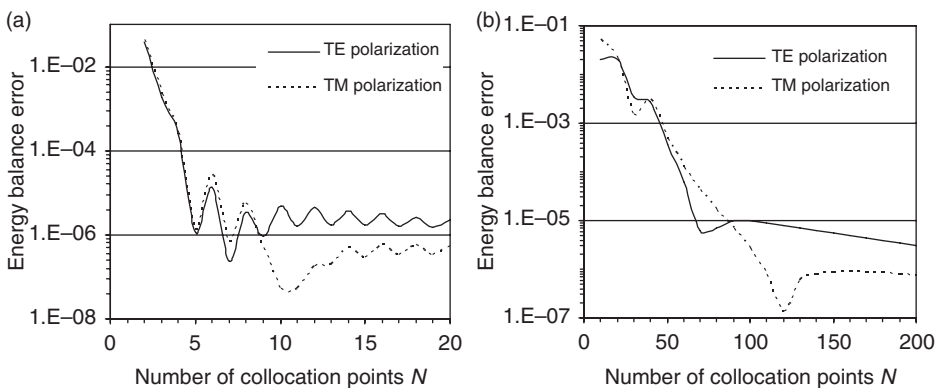


Figure 2. Numerical energy balance error with the SIM used for the problem of diffraction on a plane transmission interface (normal incidence in vacuum with the lower medium refractive index $n_1 = 1.5$) vs. number of collocation points \tilde{N} for (a) $\lambda/d = 1$ and (b) $\lambda/d = 0.1$.

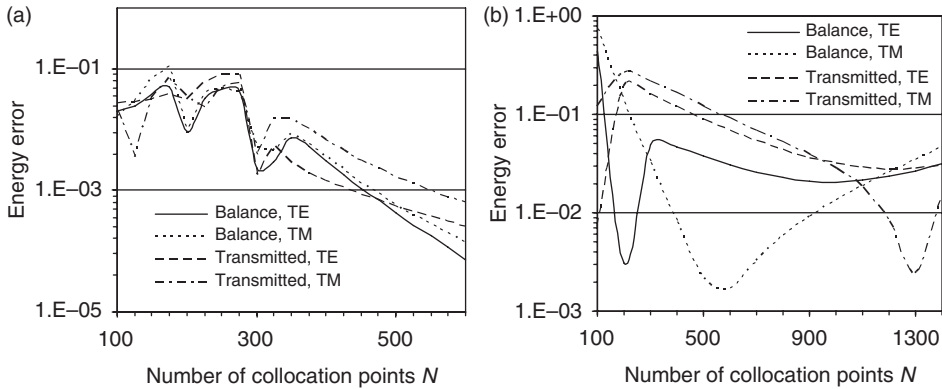


Figure 3. Numerical energy errors with the SIM vs. \tilde{N} used for the same diffraction problem as in Figure 2 but for (a) $\lambda/d=0.01$ and (b) $\lambda/d=0.001$.

For $\lambda/d = 1.E-2$ in Figure 3(a), the convergence rate, again obtained with speed-up techniques, is low with the energy balance and transmitted energy errors of $\sim 1.E-3$ in both polarizations for $\tilde{N} = 500$. The difference between the TE and TM transmitted energies for $\tilde{N} < 300$ is seen to be large, $\sim 1.E-1$. For $\lambda/d = 1.E-3$ in Figure 3(b), the convergence rate calculated with speed-up techniques is very low, with the energy balance error of $\sim 1.E-2$ in both polarizations for $\tilde{N} = 1000$. As seen from the figure, the convergence of the series deteriorates for $\tilde{N} > 1000$ as the distance between the arguments of the Green's function tends to 0. In contrast to the plots of Figure 3(b), the results for $\lambda/d = 1.E-6$ obtained without application of any speed-up techniques exhibit the fastest convergence rate with a negligible energy balance error of $\sim 1.E-16$ for $\tilde{N} = 2$ only and are equivalent to analytical calculations. The most important among the convergence speed-up options which have to be switched off in this case is the allowance for logarithmic singularity [8], and second important is the correction applied to account for the cut-off terms in the expansions of the Green's series (the Aitken δ^2 term in our case [6]).

Shallow gratings and rough mirrors exhibit similar behavior for very low λ or λ/d in the X-ray and extreme ultraviolet (EUV) ranges. While at least one collocation point per wavelength is required to reach efficiency convergence for the SIM, the MIM works reliably and fast despite the very small number of collocation points per wavelength used in the approach (it is also true for echelles [22]). For example, if a period includes 50 collocation points and $\lambda/d = 1.E-3$, there is only $5.E-2$ points per wavelength required for the MIM. In this case, however, the profile depth, the bilayer thickness, and the incident radiation wavelength must be of the same order of magnitude. The same rule for reaching the maximum diffraction efficiency is, on the whole, valid for longer wavelengths too. While the results presented in Figures 2 and 3 may certainly be different for various realizations of the integral method and of the speed-up techniques used, the overall pattern remains the same. Such calculations depend also significantly, as shown in Figure 4 and will be discussed further, on the actual summation rule chosen for Green's series.

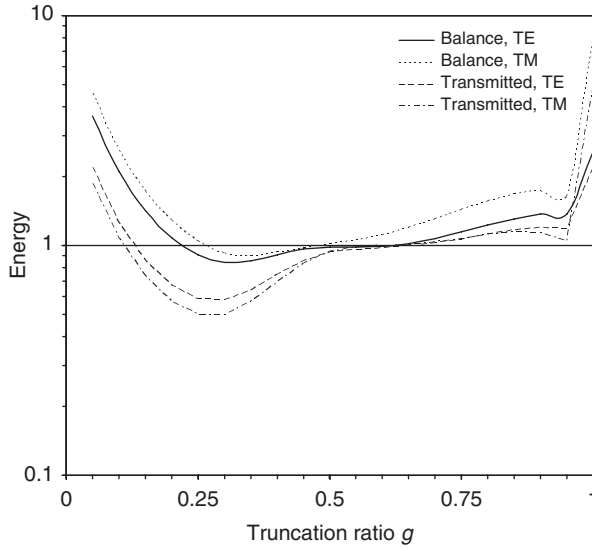


Figure 4. Energy balance and transmitted energy for calculations using the MIM vs. truncation ratio g for the same diffraction problem as in Figure 2 but for $\lambda/d=0.01$ and $\tilde{N}=100$.

3.3. Summation rule for the Green’s series

The MIM described here specifies the number of positive and negative terms in the Green’s functions and their normal derivative expansions. In the simplest case typical of real problems, the kernels are truncated symmetrically at the lower summation index $-P$ and the upper index $+P$, where P is an integer defined by

$$P \approx g\tilde{N}. \tag{21}$$

The truncation ratio g is optimized for small values of \tilde{N} and is kept constant as \tilde{N} increases. It was found that g equal to one-half is a reasonably good choice for most practical computations and, in particular, for small λ/d . Typical dependencies on g for the above example with $\lambda/d=1.E-2$ are shown in Figure 4. The energy balance is closer to 1 in both polarizations and TE/TM transmitted energies are close to each other at $g=0.5$, with divergence seen to set in at smaller and larger values of g . While today this rule is no more than empirical, there can be no doubt whatsoever that this choice is valid, and this has been verified in many realistic examples during recent years. Note that in the SIM developed in [8], $g=2/3$ for the resonance domain and should be varied for different λ/d . It is worth noting that $g=2/3$ is worse than $g=1/2$ because the computation time is proportional to $2P\tilde{N}^2$. Significantly, the number of positive and negative exponential terms used in computations of the Green’s functions and their normal derivatives should be restricted to be not larger than \tilde{N} , because such series diverge for $P \geq \tilde{N}$ [2,8,21].

Instead of the direct summation algorithm used in the MIM, more sophisticated methods can be implemented to accelerate the computation of the integral kernels in

the SIMs (cf. e.g. [12]). Unfortunately, it has turned out that such approaches are not efficient for very small λ/d problems. To reduce computing time for matrices of the discretized operator equations, two enhancements at the algorithmic level are used in the MIM: cache for the Green's series and cache for exponential functions (plane waves) [2]. Both assume a big time–memory trade-off at small λ/d . The amount of memory required for cache can be calculated in advance in each case and adjustments (cache off or partial) are done automatically.

One more important note regarding the energy balance summation appears to be pertinent here. The Green's function and its derivative members tend to big values when the y -component β_m^{\mp} of the m -th diffraction order wavevector in the upper medium or/and in the lower medium (for transmission gratings) tends to zero. This means that the diffraction order becomes grazing or even close to evanescent. Its efficiency may be high from the physical point of view or/and diverge from the mathematical point of view (it depends also on \tilde{N}). It is well known from diffraction theory that the efficiency of strictly grazing propagating, as well as of all evanescent, orders is zero. Moreover, various rigorous and approximate methods valid for shallow gratings operating at small λ/d , as well as all experimental data suggest convincingly that the efficiency decreases rapidly with increasing modulus of the diffraction order number. As a rule, the efficiencies of such grazing orders are very close to zero and much less than the accuracy of computations. Thus, such big efficiencies which correspond to high grazing orders must be excluded from the energy balance considerations.

4. Different physical models and sample calculations

Three types of small λ/d problems are known from optical applications: (a) shallow gratings working in the X-ray and EUV ranges, both at near-normal and grazing angles; (b) deep echelle gratings with a steep working facet illuminated along its normal by light of any wavelength; and (c) rough mirrors and gratings in which rough boundaries can be represented by a large- d grating, and which contain a number of random asperities illuminated at any possible angle and wavelength. Different representations of border profiles accounting for their shape and conductivity types can be utilized to compute efficiencies of such various relief structures.

To study the scattering intensity with the use of a forward electromagnetic code and Monte Carlo simulation, one should first of all prepare statistical realizations of the boundary profiles of the structure under investigation, then calculate the scattering intensity for each realization and, finally, average the intensities over all the realizations. The present author used the spectral method [23] to generate plane surfaces with a Gaussian height distribution and a Gaussian correlation function. To allow randomization of grating boundaries, this method was extended to include the case of non-plane interfaces prescribed by arbitrary polygons [7]. Non-plane boundaries are characteristic also of self-assembled low-dimensional quantum structures defined by other asperity statistics. For an investigation of specular and

diffuse X-ray scattering from multiple ensembles of quantum dots in the frame of MIM, the reader is referred to [24].

A few words regarding the extent to which the calculations made in extremely hard cases can be trusted are in order here. The workability of the programs has been confirmed by numerous tests usually employed in non-extreme cases, more specifically, the reciprocity theorem, stabilization of results under doubling of \tilde{N} and variation of g , comparison with analytically amenable cases of plane interfaces, consideration of the inverse (non-physical) radiation condition, insertion of fictitious boundaries of various geometries in layers, use of different variants of collocation point distribution and shifts, comparison with the results obtained by another of our codes or with published data, or with information corresponded to us by other researchers, including results of measurements.

4.1. Real border profile Mo/Si multilayer grating for unpolarized near-normal-incident EUV

An example of efficiency calculations for cases (a) and (c) combined is presented in Figure 5; it is essentially a 20-pair Mo/Si-coated 4200 groove/mm flight grating of the solar mission *Hinode* (former *Solar-B*) working in the 17–22-nm wavelength range [1]. The real border profile of the grating as measured by atomic force microscopy had trapezoidal shape with a 6-nm groove depth, 35° slopes, and random roughnesses, which required application of randomization to a trapezoid to allow exact efficiency prediction. Three different physical models can be applied to compute efficiencies of such a complex grating structure: the ‘rigorous’ one taking

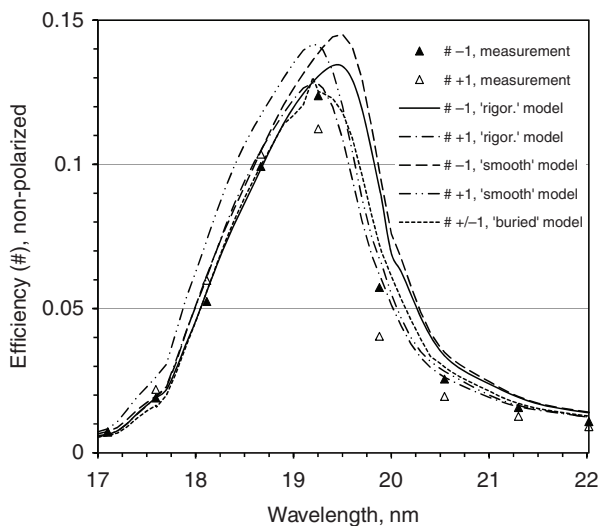


Figure 5. Calculated and measured ± 1 st order non-polarized efficiencies of the 4200/mm grating with 20 Mo/Si bilayers on Si, which operates at an angle of incidence of 6.5° vs. wavelength.

into account 41 randomly rough trapezoidal borders; the ‘smooth’ model taking into account 41 perfect trapezoidal borders; and the ‘buried’ model with 40 upper plane borders plus one bottom perfect trapezoidal border, and Debye–Waller (DW) amplitude factors allowing for random roughnesses on plane interfaces [5,25]. For the ‘rigorous’ model the trapezoidal interface has rms roughness $\sigma = 0.2$ nm (Si–Mo) and $\sigma = 0.85$ nm (Mo–Si) and lateral correlation length $\zeta = 10$ nm. It is worth noting that the ‘buried’ model, with a stack of plane interfaces over one non-planar interface, can be used to advantage, due to its good accuracy and very high speed, for multilayer grating efficiency predictions for shallow gratings in X-ray–EUV ranges [1,3,6]. As the depth of modulation and the wavelength decrease, the problem with plane interfaces becomes a good physical approximation to the model with identical non-planar borders. There are no mathematical approximations in this model except the numerical implementation.

The ‘rigorous’ and the ‘buried’ models are capable of accurately predicting both the shape of the efficiency curves and the heights of their maxima (see Figure 5). While the physical model utilizing one non-plane border and the DW asymptotic to allow for roughnesses does not yield wavelength separation of the inside (plus) and outside (minus) orders, the ‘rigorous’ and ‘smooth’ models are capable of accurately predicting the position of the efficiency maxima. Thus, the ‘rigorous’ model is the best model which gives efficiencies close to measured data. Five sets of 41 generated rough non-correlated border profiles are enough to compute exact efficiencies of such a multilayer grating with the energy balance error of $\sim 1.E-4$ for $\tilde{N} = 100$. None of the known convergence speed-up techniques have been applied in all cases. The time taken up by one ‘rigorous’ computation on a workstation with two Quad-Core Intel® Xeon® 2.66 GHz processors, 8 MB L2 Cache, 1333 MHz Bus Clock and 16 GB RAM, is about six seconds when operating under Windows Vista® Ultimate 64-bit and employing eightfold paralleling.

4.2. Oxidized Al echelle for TE/TM polarization in the near ultraviolet

As to case (b), for echelles, in which resonance on the working facet plays a predominant role, it is often, but not always, possible to ‘rotate’ a plane stack in the ‘buried’ model and consider an incidence on the grating coating with respect to the working facet rather than to the substrate [3,6]. This approach generally works in the case of thin layers (layer thickness-to-wavelength < 0.1), an area hard to cope with for SIMs. However, the sophisticated approach developed for single-coated echelles in [12] is fast and exhibits a high rate of convergence. Figure 6 displays an example from the above publication which calculated the TE/TM -122 order efficiency and absorption (IESMP data) for an 83-groove/mm, 78.7° coated aluminum echelle in the Littrow mount at λ of 193 nm vs. thickness of the natural protective Al_2O_3 layer, and compared the calculations with the data obtained with our ‘buried’ model.

The efficiency results presented for the TM polarization are close in the whole thickness range. For the TE polarization, the agreement within a few percent in the efficiency is reached for layer thicknesses less than ~ 15 nm. The energy balance error

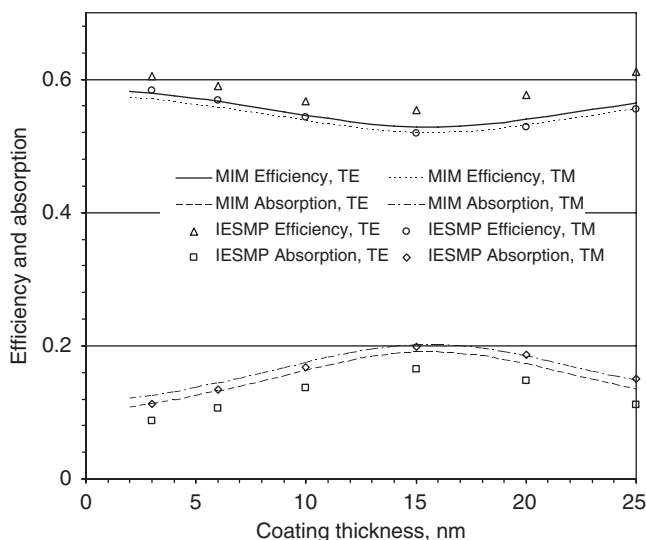


Figure 6. -122 order TE and TM efficiencies and absorptions calculated for an 83-groove/mm, 78.7° Al echelle in Littrow mount at $\lambda = 193$ nm vs. Al_2O_3 -coated layer thickness.

reached in both polarizations is $\sim 1.E-4$ for $\tilde{N} = 600$. Note that the convergence speed-up techniques were used in this deep grating case. The time taken up by one computation on the above-mentioned workstation is about seven seconds.

4.3. Rough Au mirror for TE-polarized grazing incidence X-rays

A bulk model of a typical gold X-ray mirror for use at grazing incidence near the angle of total external reflection was chosen as an example of case (c). The difference between the asymptotic and rigorous approaches can be clearly seen in Figure 7(a) which plots the calculated specular TE reflectivity of Au surfaces with $\sigma = 1.5$ nm vs. the grazing angle of incidence for Cu K_{α_1} radiation ($\lambda = 0.154$ nm) and for different values of ζ . The reflection coefficients calculated rigorously in the low-intensity domain for $\zeta = 10 \mu\text{m}$ are approximately twice those obtained with the DW asymptotics (Born approximation) which is commonly used in this region and corresponds to $\zeta = \infty$. For $\zeta = 0.1 \mu\text{m}$, the excess is already about fourfold. By contrast, close to the critical angle (Figure 7b) the rigorous data obtained for $\zeta = 0.1 \mu\text{m}$ lie $\sim 20\%$ below the values calculated for this region with the Nevot-Croce factor [25], which corresponds to $\zeta = 0$ and is derived in the frame of the first-order distorted-wave Born approximation (DWBA) [5]. For $\zeta = 10 \mu\text{m}$, in the region of high intensities, the differences are still larger, to reach finally a few hundred percent.

The behavior of the scattering intensity on ζ which is illustrated graphically in Figure 7 matches qualitatively with the results obtained in the frame of the second-order DWBA while differing clearly in quantitative estimates, particularly for values

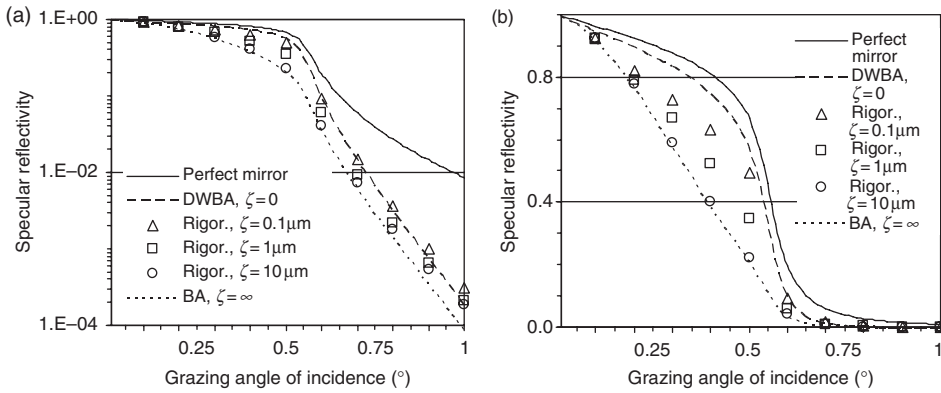


Figure 7. Specular TE reflectance of Au surfaces calculated for rms roughness $\sigma=1.5$ nm and different correlation lengths ζ for $\lambda=0.154$ nm vs. grazing angle of incidence on (a) logarithmic and (b) linear scales.

of ζ for which second-order DWBA does not work [26]. To reach the required average statistical depth with due allowance for the fine structure of the roughness in the above example, one has to use ~ 100 asperities per d , average over 9–25 random boundaries and assume 400–3200 collocation points. For $\zeta=10\mu\text{m}$ and $d=1500\mu\text{m}$, $\lambda/d\approx 1.E-7$, a value too small to be dealt with in any known rigorous numerical approach. For the MIM, however, this formidable scattering problem is found to be convergent and yields quite accurate results (energy balance error $\sim 1.E-6$) for only 400 collocation points used and no speed-up techniques invoked. The time taken up by one computation on the above mentioned workstation is about eight seconds.

5. Summary

The boundary integral equation method was considered for small wavelength-to-period 2D diffraction problems. A few principally important areas of its modification were pointed out. Special attention was paid to the main aspects of the MIM for $\lambda/d\ll 1$ as well as to a more general treatment of the energy conservation law applicable to multilayer absorption gratings.

In the cases of shallow gratings and mirrors working at very small λ/d , introducing speed-up terms in boundary integral equation methods produces an adverse numerical effect because of the ensuing uncontrolled growth of coefficients in analytically improved asymptotic estimations. With all speed-up options turned off, it is possible to obtain, for the most difficult problems, surprisingly good convergence in orders of practical interest, and an energy balance very close to 1.

The developed MIM works reliably and fast for very low λ or λ/d in the X-ray–EUV range, despite the small number of collocation points per wavelength used in the approach; however, the profile depth, the bilayer thickness, and the incident radiation wavelength must be of the same order of magnitude. It is also true for echelles working at any wavelength.

The accurate results obtained by the rigorous method for the intensity of X-ray scattering by rough mirrors and randomly rough gratings may differ substantially from those derived using known asymptotics and approximate approaches. These differences may give rise, for instance, to incorrect estimates of the rms roughness and correlation length if they are determined by comparing experimental data with calculations. Besides, the rigorous approach permits taking into account any known roughness statistics.

Acknowledgements

The author feels indebted to Sergey Sadov (Newfoundland Memorial University, Canada) for the information provided and fruitful collaboration. Helpful discussions and testing with Bernd Kleemann (Carl Zeiss AG, Germany), Andreas Rathsfeld (WIAS, Germany), and Gunther Schmidt (WIAS, Germany) are greatly appreciated.

References

- [1] L.I. Goray, J.F. Seely, and S.Yu. Sadov, *Spectral separation of the efficiencies of the inside and outside orders of soft-X-ray-extreme ultraviolet gratings at near normal incidence*, J. Appl. Phys. 100 (2006), 094901.
- [2] L.I. Goray, I.G. Kuznetsov, S.Yu. Sadov, and D.A. Content, *Multilayer resonant subwavelength gratings: Effects of waveguide modes and real groove profiles*, J. Opt. Soc. Am. A 23 (2006), pp. 155–165.
- [3] L.I. Goray, *Numerical analysis of the efficiency of multilayer-coated gratings using integral method*, Nucl. Instrum. Meth. A 536 (2005), pp. 211–221.
- [4] M.V. Babich and V.S. Buldyrev, *Asymptotic Methods in Short-wavelength Diffraction Theory, Alpha Science Series on Wave Phenomena*, Oxford University Press, Oxford, 2007.
- [5] T.M. Elfouhaily and C.-A. Guerin, *A critical survey of approximate scattering wave theories from random rough surfaces*, Waves Random Media 14 (2004), pp. R1–R40.
- [6] L.I. Goray and S.Yu. Sadov, *Numerical modeling of coated gratings in sensitive cases*, OSA TOPS 75 (2002), pp. 365–379.
- [7] See website at www.pcgrate.com.
- [8] D. Maystre, *Integral methods*, in *Electromagnetic Theory of Gratings*, R. Petit, ed., Springer, Berlin, 1980, pp. 53–100.
- [9] L.I. Goray and G. Schmidt, *Solving conical diffraction grating problems with integral equations*, J. Opt. Soc. Am. A 27 (2010), pp. 585–597.
- [10] A. Pomp, *The integral method for coated gratings: Computational cost*, J. Mod. Opt. 38 (1991), pp. 109–120.
- [11] L.I. Goray, *Specular and diffuse scattering from random asperities of any profile using the rigorous method for X-rays and neutrons*, Proc. SPIE 7390 (2009), 73900V.
- [12] A. Rathsfeld, G. Schmidt, and B.H. Kleemann, *On a fast integral equation method for diffraction gratings*, Commun. Comput. Phys. 1 (2006), pp. 984–1009.
- [13] B. Kleemann, A. Mitreiter, and F. Wyrowski, *Integral equation method with parametrization of grating profile: Theory and experiments*, J. Mod. Opt. 43 (1996), pp. 1323–1349.

- [14] D. Maystre, M. Neviere, and R. Petit, *Experimental verifications and applications of the theory*, in *Electromagnetic Theory of Gratings*, R. Petit, ed., Springer, Berlin, 1980, pp. 159–225.
- [15] L.I. Goray and J.F. Seely, *Efficiencies of master replica, and multilayer gratings for the soft-X-ray–extreme-ultraviolet range: Modeling based on the modified integral method and comparisons with measurements*, *Appl. Opt.* 41 (2002), pp. 1434–1445.
- [16] B.H. Kleemann and J. Erxmeyer, *Independent electromagnetic optimization of the two coating thicknesses of a dielectric layer on the facets of an echelle grating in Littrow mount*, *J. Mod. Opt.* 51 (2004), pp. 2093–2110.
- [17] M. Neviere and E. Popov, *Light Propagation in Periodic Media: Differential Theory and Design*, Marcel Dekker, New York, 2002.
- [18] E. Popov, B. Bozhkov, D. Maystre, and J. Hoose, *Integral method for echelles covered with lossless or absorbing thin dielectric layers*, *Appl. Opt.* 38 (1999), pp. 47–55.
- [19] B.H. Kleemann, J. Gatzke, Ch. Jung, and B. Nelles, *Design and efficiency characterization of diffraction gratings for applications in synchrotron monochromators by electromagnetic methods and its comparison with measurement*, *Proc. SPIE* 3150 (1997), pp. 137–147.
- [20] M. Saillard and D. Maystre, *Scattering from metallic and dielectric surfaces*, *J. Opt. Soc. Am. A* 7 (1990), pp. 982–990.
- [21] L.I. Goray, *Modified integral method for weak convergence problems of light scattering on relief grating*, *Proc. SPIE* 4291 (2001), pp. 1–12.
- [22] L.I. Goray, *Modified integral method and real electromagnetic properties of echelles*, *Proc. SPIE* 4291 (2001), pp. 13–24.
- [23] L. Tsang, J.A. Kong, K.-H. Ding, and C.O. Ao, *Scattering of Electromagnetics Waves: Numerical Simulations*, John Wiley, New York, 2001.
- [24] L.I. Goray, N.I. Chkhalo, and G.E. Cirilin, *Determination of facet angles and heights of quantum dots from the analysis of diffuse and specular X-ray scattering*, *Technical Phys.* 79 (2009), pp. 117–124.
- [25] E. Spiller, *Soft X-ray Optics*, SPIE Press, Bellingham, 1994.
- [26] D.K.G. de Boer, *Influence of the roughness profile on the specular reflectivity of X-rays and neutrons*, *Phys. Rev. B* 49 (1994), pp. 5817–5820.